

AD-753 707

ANALYSIS OF ELECTRON BEAM IRRADIATION OF  
THE UPPER ATMOSPHERE

Fritz Bien

Aerodyne Research, Incorporated

Prepared for:

Rome Air Development Center  
Advanced Research Projects Agency

September 1972

DISTRIBUTED BY:

**NTIS**

National Technical Information Service  
U. S. DEPARTMENT OF COMMERCE  
5285 Port Royal Road, Springfield Va. 22151

# DISCLAIMER NOTICE

THIS DOCUMENT IS THE BEST  
QUALITY AVAILABLE.

COPY FURNISHED CONTAINED  
A SIGNIFICANT NUMBER OF  
PAGES WHICH DO NOT  
REPRODUCE LEGIBLY.

IRADC-TR-72-297  
Final Technical Report  
October 1972



## ANALYSIS OF ELECTRON BEAM IRRADIATION OF THE UPPER ATMOSPHERE

Aerodyne Research, Inc.

Sponsored by  
Defense Advanced Research Projects Agency  
ARPA Order No. 1649

Approved for public release;  
distribution unlimited.



The views and conclusions contained in this document are those of the authors and should not be interpreted as necessarily representing the official policies, either expressed or implied, of the Defense Advanced Research Projects Agency or the U.S. Government.

Reproduced by  
NATIONAL TECHNICAL  
INFORMATION SERVICE  
U S Department of Commerce  
Springfield VA 22151

Rome Air Development Center  
Air Force Systems Command  
Griffiss Air Force Base, New York

AD753707

~~UNCLASSIFIED~~  
~~Security Classification~~

DOCUMENT CONTROL DATA - R & D

(Security classification of title, body of abstract and indexing annotation must be entered when the overall report is classified)

1. ORIGINATING ACTIVITY (Corporate Author) Aerodyne Research, Inc. Northwest Industrial Park Burlington, Massachusetts		2a. REPORT SECURITY CLASSIFICATION Unclassified	
3. REPORT TITLE Analysis of Electron Beam Interaction with the Upper Atmosphere		2b. GROUP	
4. DESCRIPTIVE NOTES (Type of report and inclusive dates) Research Report 2/15/72 - 9/14/72			
5. AUTHOR(S) (First name, middle initial, last name) Fritz Blen			
6. REPORT DATE September 1972	7a. TOTAL NO. OF PAGES 51 48	7b. NO. OF REFS 54	
8a. CONTRACT OR GRANT NO. F30602-72-C-0271	8b. ORIGINATOR'S REPORT NUMBER(S) ARI-RR-11		
9. PROJECT NO. ARPA Order No. 1649	9b. OTHER REPORT NUMBER (Any other numbers that may be assigned this report) RADC-TR-72-297		
10. DISTRIBUTION STATEMENT Approved for public release - Distribution unlimited			
11. SUPPLEMENTARY NOTES Joseph J. Simons (315) 330-3451 RADC Griffiss AFB, New York 13440		12. SPONSORING MILITARY ACTIVITY Advanced Research Projects Agency Washington, D.C. 20301	
13. ABSTRACT A study has been made of the physics and chemistry involved when energy is deposited into the upper atmosphere by electrons. Calculations have been made both of the size and shape of the electron interaction region and of the radiation intensity produced in that region. The results of the NASA artificial aurora experiment performed by Hess et al., in 1969 has been analyzed in this context. The emission produced from electron interaction with the atmosphere in the 3500 to 8000A region has been analyzed. The size and shape of the observed region have been calculated by fitting laboratory measurements to the earth's exponential atmosphere, taking into account the geomagnetic field and are attributed to prompt radiation from N <sub>2</sub> <sup>+</sup> first negative, N <sub>2</sub> first positive, and O <sub>2</sub> <sup>+</sup> first negative, as well as to the afterglow radiation from OI 5577A and 6300A emitters. The calculated time dependence of the afterglow signal was found to be consistent with observations.			

- 1 -

**Security Classification**

**● ● ● ● ●**

1122

1. 1. 1. 1. 1.

1998

**SOLE**



595

100%



- 11 -

**Security Classification**

RADC-TR-72-297  
September 1972

ANALYSIS OF ELECTRON BEAM IRRADIATION  
OF THE UPPER ATMOSPHERE

Fritz Bien

Contractor: Aerodyne Research, Inc.  
Contract Number: F30602-72-C-0271  
Effective Date of Contract: 15 February 1972  
Contract Expiration Date: 14 September 1972  
Amount of Contract: \$45,940.00  
Program Code Number: 2E20

Principal Investigator: Dr. Morton Camac  
Phone: 617-272-1100  
Project Engineer: Joseph J. Simons  
Phone: 315-330-3451

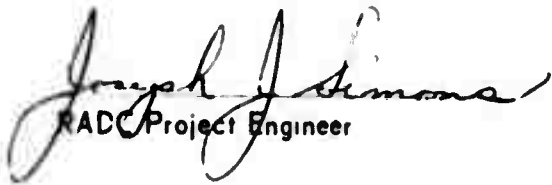
Approved for public release;  
distribution unlimited.

- iii -

This research was supported by the  
Defense Advanced Research Projects  
Agency of the Department of Defense  
and was monitored by Joseph J. Simons  
RADS (OCSE), GAFB, NY 13441 under  
contract F30602-72-C-0271.

## PUBLICATION REVIEW

This technical report has been reviewed and is approved

  
RADC Project Engineer

## TABLE OF CONTENTS

<u>Section</u>	<u>Page</u>
ABSTRACT . . . . .	iii
REPORT SUMMARY . . . . .	ix
1. INTRODUCTION . . . . .	1
2. NASA "ARTIFICIAL AURORA" EXPERIMENT . . . . .	3
3. THEORETICAL MODEL OF ELECTRON BEAM INTERACTION WITH THE ATMOSPHERE . . . . .	7
4. ATMOSPHERIC CHEMISTRY ASSOCIATED WITH ELECTRON IRRADIATION . . . . .	13
5. APPLICATION OF THE MODEL TO NASA "ARTIFICIAL AURORA" EXPERIMENT . . . . .	23
6. DISCUSSION AND CONCLUSIONS . . . . .	33
REFERENCES . . . . .	37



## LIST OF ILLUSTRATIONS

<u>Figure</u>		<u>Page</u>
1	Sketch of the Electron Beam Accelerator Trajectory and the Magnetic Field Orientation Described by Davis (1971) . . . . .	3
2	Relative Response of the S-20 Photocathode Multiplier and Lens Transmittance (Taken from Davis et al., 1971) . . . . .	4
3	Energy Deposition as a Function of Distance Away From the Electron Beam for Constant Density and No Magnetic Field . . . . .	9
4	Diffusion Coefficient at Different Altitudes (Taken From Keneshca and Zimmerman (1970)) . . . . .	21
5	Ion Production Rate With Respect to Altitude Calculated for Conditions of the NASA Experiment . . . . .	23
6	Sketch of the Electron Irradiated Region as the Electron Accelerator Moves Through the Atmosphere . . . . .	26
7	Steady-State Emission Levels From Prompt Radiators in the 3500 to 8000A Region . . . . .	27
8	Calculated Emission Intensities From $O(^1S)$ and $O(^1D)$ During Electron Irradiation at 106 km Altitude . . . . .	28
9	Calculated Emission Intensities From $O(^1S)$ and $O(^1D)$ During Electron Irradiation at 110 km Altitude . . . . .	28
10	Calculated Emission Intensities From $O(^1S)$ and $O(^1D)$ During Electron Irradiation at 120 km Altitude . . . . .	28
11	Emission Intensity of Afterglow Radiation From $O(^1S)$ and $O(^1D)$ After 0.67 Sec Irradiation Time, 106 km Altitude . . .	29
12	Emission Intensity of Afterglow Radiation From $O(^1S)$ and $O(^1D)$ After 0.67 Sec Irradiation Time, 110 km Altitude . . . . .	29

## LIST OF ILLUSTRATIONS (Cont.)

<u>Figure</u>		<u>Page</u>
13	Emission Intensity of Afterglow Radiation From O( <sup>1</sup> S) and O( <sup>1</sup> D) After 0.67 Sec Irradiation Time, 120 km Altitude . . . . .	30
14	5577A OI Emission for O( <sup>1</sup> S) Produced by: <div style="display: flex; justify-content: space-between; margin-top: 5px;"> <div style="width: 45%;">                     (1) <math>O_2^+ + e \rightarrow O + OI(^1S)</math>;                      (2) <math>O + N_2(A) \rightarrow O(^1S) + N_2</math>;                      (3) <math>O + e \rightarrow O(^1S) + e</math>; </div> <div style="width: 45%;">                     (4) <math>(O_2 + e \rightarrow O + O(^1S) + e</math>;                      Case (a) for <math>\sigma = 1.5 \times 10^{-19}</math>,                      Case (b) for <math>\sigma = 1 \times 10^{-16}</math> . . . </div> </div>	31

## REPORT SUMMARY

The objective of this project is to investigate the effects of using an electron beam to artificially disturb the upper atmosphere, thus simulating natural disturbances such as auroras. This report involves both a general study of the effects of electron radiation on the upper atmosphere and the specific application of these effects to an experiment performed by the National Aeronautic and Space Administration.

The purpose of this paper is to present an analysis of electron beam interaction with the upper atmosphere. In order to better understand the phenomenology that would be involved when the atmosphere is artificially excited by an electron beam, specific aspects of an experiment performed by Hess et al. (1970) are analyzed. Electron beam spreading, energy deposition, and penetration are studied. Reactions involving air chemistry and radiation which result from this interaction are also studied. Information from the NASA "artificial aurora" experiment has been analyzed and compared to the results of this study.

The study is reported in three parts: the spreading and penetration of an electron beam in the upper atmosphere, together with the effects of the motion of the beam accelerator are discussed in Section 3. The atmospheric chemistry that is involved due to the electron interaction is discussed in Section 4. Finally, these calculations are compared with NASA observations in Section 5. While the NASA data was quite limited, the description presented of the electron irradiation of the upper atmosphere is in good agreement with these data.

The width of the electron cloud as well as the energy deposition has been adequately modeled by this analysis. The effects of the geomagnetic field

strength and orientation has been included. The altitudes at which electrons deposit most of their energy is a function of the initial electron energy. This penetration has been modeled by taking into account atmospheric density variation with altitude. Using this formulation, calculations of the energy deposited as a function of altitude have been made which show good agreement with observed data.

The chemistry and radiation involved due to electron irradiation has been studied in detail. A complete description of the visible emission involved is presented. This calculated emission is in good agreement with that observed, both in intensity and in temporal behavior. With this agreement, confidence has been gained for predicting the emission intensities during both natural and man-made disturbances of the upper atmosphere.

## SECTION I

### INTRODUCTION

Upper atmospheric phenomena during quiescent and disturbed conditions are presently under intensive study. Ground-based (Donahue, 1971), airborne (Stair and Gavrin, 1967) and rocketborne (Snider and Narcisi, 1970) platforms have obtained E-region measurements of electron and ion-density profiles (Donahue et al., 1970; Feldman et al., 1971a), concentrations of minor species and metastables (Zipl et al., 1970), and radiation from these species (Donahue, 1966; Parkinson et al., 1970b). Theoretical calculations have shown that ion-concentration measurements during quiescent conditions are in excellent agreement with steady state chemistry and radiation calculations (Donahue, 1966; Ulwick, 1967; Donahue, 1968a). However, much less is understood during atmospheric disturbances, such as auroras.

Measurements taken from ground- and aircraft-based instruments of the radiation emitted during auroral activity have shown rapid temporal variations in the radiative intensities. However, these measurements have been unable to locate the precise altitude of the radiating species (Chamberlain, 1961; Donahue, 1971). Rocket-borne measurements, on the other hand, have yielded information on the altitude dependence of the radiating species (Snider and Narcisi, 1970; Feldman et al., 1971a) but only very limited information on temporal variations. Such have also been launched mainly into the quiet post break-up stage of auroral activity.

A complimentary technique to these direct measurement programs is to artificially create an auroral type disturbance as has been proposed by Stair (1971). Using this technique, an artificial aurora would be produced by launching a high-altitude probe with an onboard electron-beam system to irradiate the atmosphere with electrons. An experiment similar to this proposal was performed by NASA in 1969 (Hess et al., 1971; Davis et al., 1970, 1971). A rocket

containing an electron beam accelerator was used to create an artificial upper atmospheric disturbance to test a scheme for mapping geomagnetic field lines. The electron beam was directed downward along the magnetic field and the radiation was observed along columns about 130 meters wide extending from 104 to 130 km in altitude. Additional details regarding this experiment are presented in the next section.

The present study develops a theoretical model for the electron-beam interaction with the atmosphere. The analysis includes a description of the shape and extent of the interaction region, the atmospheric ionization levels and the chemistry and radiation following the electron irradiation. This model is treated in detail in Sections 2 and 4. Specific calculations of the atmospheric interaction under the conditions of the NASA experiment are performed using this model. In Section 5, the intensity and time dependence of the visible radiation are calculated and compared to the observations made in the NASA experiments. Particular interest is paid to the mechanism for producing  $O(^1S)$  radiation which was found in the experiments to persist after electron-beam irradiation had ceased.

## SECTION 2

### NASA "ARTIFICIAL AURORA" EXPERIMENT

On January 26, 1969, at 9:45 UT (4:45 A.M., EST), an Aerobee 350 rocket carrying an electron beam accelerator was launched from Wallops Island, Virginia. The rocket trajectory had an azimuth  $97^{\circ}$ , reaching an apogee of 269 km at a distance 27 km east of the launch point. Near apogee, the rocket was maneuvered so that the onboard electron gun directed the beam downward along the geomagnetic field. The relation between the rocket trajectory and the magnetic field, which had a local inclination of  $69.5^{\circ}$  and a declination of  $-8^{\circ}$  is shown in Figure 1.

The electron beam accelerator commenced operation 206 sec after launch. A 21 pulse sequence, each consisting of a pulse every 2.7 sec, was repeated for 252 sec. The pulse voltages and currents were varied from 1 to 8.7 kV and from 1.5 to 490 ma, respectively. Pulse duration was either 0.1 sec or 0.98 sec. The strongest pulse (numbers 11 and 21 in the pulsing sequence) were operated at 490 ma and 8.7 kV for 0.98 sec. Four of these pulses were observed before the electron beam accelerator passed out of the view of the ground-based detectors. On closer examination of the data, one additional trace operating at 490 ma, 4.9 kV, for 0.1 sec was also observed.

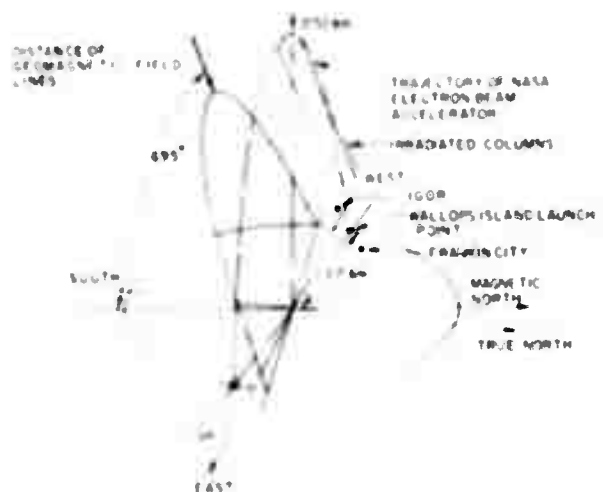


Figure 1. Sketch of the Electron Beam Accelerator Trajectory and the Magnetic Field Orientation Described by Davis (1971)

Measurements on the irradiated region were made from ground-based stations located at Franklin City and Igor using image-orthicon systems with a framing speed of 30 frames per second. Figure 2 shows the response curve for the S-20 photocathode image orthicon and lens system (Davis et al., 1970). The detection sensitivity of this system was estimated to be 500 rayleighs at the peak of the response curve.

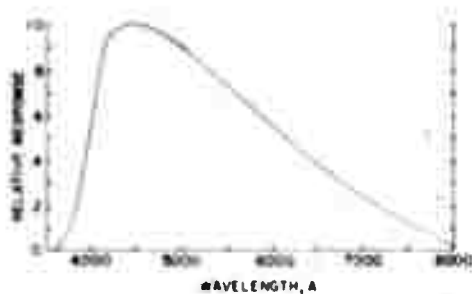


Figure 2. Relative Response of the S-20 Photocathode Multiplier and Lens Transmittance (Taken From Davis et al., 1971)

The signals recorded during the experiment are presented in Table 1. The radiation was observed from narrow tubes extending from 104 to 130 km in altitude. The measured apparent width was 60 to 240 meters with an average of about 130 meters. The column brightness while the electron beam was on was estimated to be approximately 10 to 15 kilo-rayleighs after correcting for instrument sensitivity and was due mainly to  $N_2^+$  first negative radiation. The total radiation was observed for approximately  $1.36 \pm 0.07$  sec, 0.38 sec longer than the 0.98 sec irradiation time.



TABLE 1

OBSERVED WIDTH AND UPPER AND LOWER ALTITUDES OF SIGNATURE PULSES

	ALTITUDE AT TOP, km	ALTITUDE AT BOTTOM, km	WIDTH meters
<b>FRANKLIN CITY</b>			
1st Signature	127 - 133	105.9	120
2nd Signature	130 - 138	105.5	126
3rd Signature	123 - 131	113.7	---
4th Signature	137.5	108.6	132
<b>IGOR</b>			
1st Signature	123.2	104.1	123
2nd Signature	125.3	103.9	(64)
3rd Signature	126 - 128	103.6	117
4th Signature	128.1	104.5	54

### SECTION 3

## THEORETICAL MODEL OF ELECTRON BEAM INTERACTION WITH THE ATMOSPHERE

Previous studies of electron interaction with the upper atmosphere have been performed with particular emphasis on the relationship to auroral activity. Calculations of ionization profiles due to electron excitation have been made by Chamberlain (1961). The interaction of a single collimated electron beam with the upper atmosphere, which is analyzed here, presents a somewhat more manageable problem. This model, moreover, is directly applicable to the NASA electron beam experiment.

The various effects of the electron beam interaction with the upper atmosphere can be modeled by laboratory measurements. These effects include atmospheric density variations, the magnetic field, and chemical and radiative processes following the irradiation. Experimental data on electron interaction with air has been obtained in the laboratory by Grün (1957) and by Cohn and Caledonia (1970).

The energy deposited into the upper atmosphere by an electron beam has been calculated by Berger et al. (1970) whose purpose was to describe electron transport from very high altitudes into the upper atmosphere as in the case of auroral activity. Using the Monte Carlo technique, they calculated the spread of a beam of monoenergetic electrons, injected downward from 300 km along the magnetic field, as a function of altitude. A vertical magnetic field strength of 0.6G was assumed. Under the conditions of constant density and the absence of a magnetic field, their calculations were in good agreement with laboratory measurements. A simplified formulation of this problem based on their results is presented here to facilitate analysis of the chemistry and radiation.

**Preceding page blank**

In the absence of a magnetic field, the energy deposition in air by an electron beam is nearly spherical in shape, its diameter being determined by both the electron energy and air density. The range of the beam measured by Grün (1957) was found to fit the relation

$$\text{Range} = 9.2 \times 10^{16} E_0^{7/4} n^{-1} \text{ cm} \quad (1)$$

for constant air density in the energy range between 2 and 40 keV. Here,  $E_0$  is the initial electron energy in keV and  $n$  is the number density per  $\text{cm}^3$ . For application to the atmosphere with varying density, Equation (1) must be modified to

$$\int_{s_0}^{s_f} n(s) ds = 9.2 \times 10^{16} E_0^{7/4} \quad (2)$$

where  $s_0$  is the position of the electron beam accelerator,  $s_f$  is the end of the electron beam range, and  $n(s)$  is the atmospheric number density along the path  $s$ , in our case, along the magnetic field. For a given  $n(s)$ ,  $s_f$  is determined numerically using Equation (2).

From both laboratory measurements (Grün, 1957; Cohn and Caledonia, 1970) and theoretical calculations (Berger et al., 1970; Spencer and Coyne, 1962), the spatial distribution of energy deposition has been found to be independent of the electron beam energy. The energy deposition along the initial beam direction,  $T(z/L)$ , is plotted as a function of  $z/L$  in Figure 3. Here,  $z$  is the particle thickness in units of molecules per unit area, and  $L$  is the beam range in molecules per unit area. The energy deposited at negative  $z/L$  is due to backscattered electrons. The quantity  $T(z/L)$  is normalized by the relation

$$\int_{-\infty}^{\infty} T(z/L) d(z/L) = 1 \quad .$$

The normalized particle thickness is hence defined as

$$z/L = \frac{\int_{s_0}^s n(s) ds}{\int_{s_0}^{s_f} n(s) ds} = \frac{\int_{s_0}^s n(s) ds}{9.2 \times 10^{16} E_o^{7/4}} \quad (3)$$

Thus, for a constant density gas,  $z/L$  reduces to a simple dimensionless distance with  $L$  defined by Equation (1).

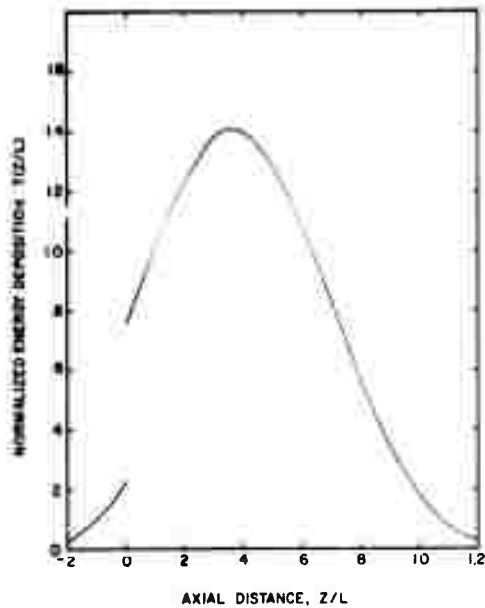


Figure 3. Energy Deposition as a Function of Distance Away From the Electron Beam for Constant Density and No Magnetic Field

Consider the case in which the electron beam is initially directed along a magnetic field. Electrons scattered perpendicular to the magnetic lines of force are turned by the field and the spherical shaped cloud is thus narrowed to a column. The range and energy distribution along the field do not change and are still represented by Figure 3. Electrons that are scattered by the atmosphere receive a velocity component perpendicular to the magnetic field and thus make circular (or spiral) orbits around the field lines. These orbits have a Larmor radius:

$$R_L = \frac{m_e c v_{\perp}}{qB} \quad (4)$$

where  $q$  and  $m_e$  are the electron charge and mass, respectively;  $B$  is the magnetic field;  $c$  is the velocity of light; and  $v_{\perp}$  is the component of velocity perpendicular to the magnetic field. In terms of the electron energy,  $E$ ,

$$R_L = \frac{c \sin \theta}{qB} (2m_e E)^{1/2} \quad (5)$$

where  $\theta$  is the angle between the direction of the motion of the electron and the magnetic field. In the vicinity of Wallops Island,  $B = 0.6$  gauss, and  $R_L$  becomes

$$R_L = 1.7 \sin \theta E^{1/2} \text{ meters} \quad (6)$$

where  $E$  is expressed in keV. For the case in which the mean free path between collisions is larger than the Larmor radius, the lateral spreading of the beam  $S_{\perp}$  is approximated by the relation

$$S_{\perp} = 2 \bar{R}_L (\text{number of collisions})^{1/2} \quad (7)$$

where  $\bar{R}_L$ , the electron Larmor radius averaged over both the energy during slowdown and the angle  $\theta$ , is approximately

$$\bar{R}_L = 1.1 (E_0)^{1/2} \text{ meters} \quad (8)$$

The number of collisions that an electron encounters during slowdown is approximately (Berger et al., 1971)

$$(\text{number of collisions}) = 25.6 E_o^{3/4} . \quad (9)$$

Combining Equations (7), (8), and (9), the lateral spread becomes

$$S_{\perp} \approx 11 E_o^{7/8} \text{ meters} . \quad (10)$$

Note that for the case in which the collisional mean free path is much larger than the Larmor radius, the lateral spread is independent of the density. The electron cloud when directed along the magnetic field becomes a column with a diameter  $S_{\perp}$  at the widest point.  $z/L \approx 0.5$  .

The average energy  $W$  required to form one ion-electron pair (Landshoff et al., 1966) is

$$W = 33.73 + [5.53(E_o - E_i)^{-1/2}] \text{ eV per ion pair} \quad (11)$$

where  $E_o$  is the initial beam energy in keV, and  $E_i = 0.015$  keV is the mean ionization energy for air. The ion-pair formation rate in the atmosphere by electron beam irradiation is

$$\begin{aligned} \text{ion-pairs/cm}^3\text{-sec} &= \frac{I E_o T(z/L)}{W S_{\perp}^2} \frac{d(z/L)}{ds} \\ &= 1.86 \times 10^{-3} I E_o^{-5/2} T(z/L) \text{ n(s)} . \end{aligned} \quad (12)$$

where  $E_0$  and  $I$  are the beam voltage in kilovolts and current in amperes, respectively, and  $n(s)$  is the atmospheric number density per  $\text{cm}^3$ .

## SECTION 4

# ATMOSPHERIC CHEMISTRY ASSOCIATED WITH ELECTRON IRRADIATION

The chemistry associated with the electron beam irradiation determines the radiation observed from the ground. Consequently, in order to predict or analyze the observed signal from electron irradiation, a detailed study of the chemistry must be performed.

The beam electrons which ionize the atmosphere use the remainder of the 35 eV energy yielded in the creation of one ion pair in dissociation and in excitation of electronic, vibrational, and rotational modes. This interaction leads to reactions which produce visible radiation. The chemistry that follows the electron irradiation may be described by coupled second-order differential equations of the form

$$\frac{\partial M}{\partial t} = D \nabla^2 M + \left. \frac{\partial M}{\partial t} \right|_{\text{chem}} \quad (13)$$

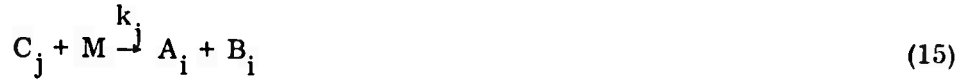
The first term on the right-hand side accounts for the diffusion effects to be discussed at the end of this section. The second denotes the change in concentration of M due to chemical reactions. This term is of primary interest in predicting the electron interaction with the upper atmosphere.

Since the altitudes at which the electrons deposit their energy (for the purposes of this analysis) are above 100 km, the chemistry consists mainly of binary reactions. Thus, to simplify the analysis, both radiation and electron interaction with the atmosphere are treated in the same form. The general reaction for producing species M is written as





where the subscript i denotes any species that is involved in forming species M and  $k_i$  is the rate constant for the reaction. The reverse reaction is written as a separate equation



with subscript j denoting a species involved in removing M. The rate constants  $k_i$  and  $k_j$  are related by the equilibrium conditions. The net change in the concentrations of species M due to chemistry becomes

$$\partial M / \partial t \big|_{\text{chem}} = \sum_i k_i [A_i][B_i] - \sum_j k_j [M][C_j] \quad (16)$$

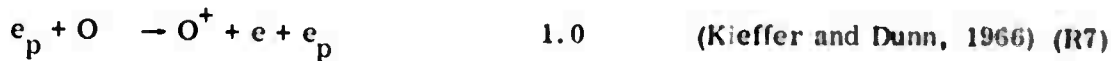
where the brackets denote the concentration of the species designated within these brackets. This binary reaction scheme has been generalized to handle from zero to three reactants and from zero to three products.

In order to treat the electron beam interaction with the atmosphere, an artificial chemical reaction with zero reactants and a production rate equal to that calculated from Equation (12) was used. This production of ion was then weighted by the relative production of each ionic species.

Reactions leading to ionization and their relative production rates are:

<u>Reaction</u>	<u>Relative Production Rate</u>	<u>Reference</u>
$N_2^+ + e + e_p$	0.75	(Landshoff et al., 1967) (R1)
$e_p + N_2 \rightarrow N^+ + N + e + e_p$	0.19	(Rapp et al., 1965) (R2)
$N_2^+ (B^2 \Sigma_u^+) + e + e_p$	0.06	(Borst and Zipf, 1970a) (R3)
$O_2^+ + e + e_p$	0.70	(Landshoff et al., 1967) (R4)
$e_p + O_2 \rightarrow O + O^+ + e + e_p$	0.29	(Rapp et al., 1965) (R5)
$O_2^+ (b^4 \Sigma_g^-) + e + e_p$	0.01	(Borst and Zipf, 1970b) (R6)

and



The subscript p denotes the fast beam electron. Reactions (R3) and (R6) illustrate examples of the production of excited states. In these cases, the ions radiate in the first negative bands



and



These radiation sources are particularly useful as their intensities are directly related to their ionization rates.

The electrons, both primary and secondary, also produce dissociation and excitation of the neutral species. The important reactions include:

Reaction	Relative Production Rate	Reference
$O_2 + e \rightarrow O(^1S) + e$	0.31	(Landshoff et al., 1967) (R10) (Barst and Zipf, 1971)
$O + e \rightarrow O(^1S) + e$	0.006	(Henry et al., 1969) (R11)
$O + e \rightarrow O(^1D) + e$	0.20	(Henry et al., 1969) (R12)
$N_2 + e \rightarrow N_2^+ + e$	0.5	(Stolarski et al., 1967) (R13)
$N_2 + e \rightarrow N + N^+ + e$	0.67	(Winter, 1966) (R14)

The atomic oxygen produced in Reaction (R10) is highly excited (Mumma and Zipf, 1971), and one half of the oxygen atoms produced in Reaction (R10) is believed to be in the  $O(^1S)$  state (Parkinson et al., 1970b, Mumma and Zipf, 1971, Feldman et al., 1971a). The main states produced in Reaction (R13) are  $N_2(C^3\Pi_u)$ ,  $N_2(B^3\Pi_g)$ , and  $N_2(A^3\Sigma_u^+)$ .

The  $N_2(C^3\Pi_u)$  and  $N_2(B^3\Pi_g)$  states decay rapidly by radiating the second and first positive band system, respectively:



in the ultraviolet, and



in the infrared and visible wavelengths. The  $N_2(A^3\Sigma_u^+)$  state is long-lived and may be a source of  $O(^1S)$  through the reaction (L. Atkinson and Zipl, 1970)



The reactions



and



are important vibrational excitation reactions which account for the secondary electron energy. Approximately 6% of the beam energy goes into vibrational excitation (Chen, 1964).

The ions produced in Reactions (R1) through (R7) undergo ionic reactions or recombine with the slow secondary electrons. The principal reactions and their rate constants (at 300 °K) are listed in Table 2. The relative rate of dissociative-recombination reactions and ion-exchange reaction substantially affects the relative concentration of the ionic species.

TABLE 2  
ION EXCHANGE REACTIONS

Reaction		*Reaction Rate (cm <sup>3</sup> /sec)	Reference	
$N_2^+$ +	$N \rightarrow N_2 + N^+$	$1 \times 10^{-11}$	(DASA, 1967)	(R20)
	$O \rightarrow NO^+ + N$	$2.5 \times 10^{-10}$	(Norton and Barth, 1970)	(R21)
	$O \rightarrow NO^+ + N(^2D)$	$7 \times 10^{-11}$	(Norton and Barth, 1970)	
	$O \rightarrow N_2 + O^+$	$1 \times 10^{-12}$	(Goldan et al., 1966)	(R23)
	$O_2 \rightarrow N_2 + O_2^+$	$3 \times 10^{-10}$	(Dunkin et al., 1968)	(R24)
	$O_2 \rightarrow NO^+ + NO$	$1 \times 10^{-17}$	(Dunkin et al., 1968)	(R25)
	$NO \rightarrow N_2 + NO^+$	$3 \times 10^{-10}$	(Goldan et al., 1966)	(R26)
$N^+$ +	$O \rightarrow N + O^+$	$1 \times 10^{-12}$	(Schmeltekopf et al., 1968)	(R27)
	$O_2 \rightarrow N + O_2^+$	$3 \times 10^{-10}$	(Dunkin et al., 1968)	(R28)
	$O_2 \rightarrow NO^+ + O$	$3 \times 10^{-10}$	(Dunkin et al., 1968)	(R29)
	$O_2 \rightarrow O + NO$	$1 \times 10^{-12}$	(DASA, 1967)	(R30)
	$NO \rightarrow N + NO^+$	$8 \times 10^{-10}$	(Dunkin et al., 1968)	(R31)
	$NO \rightarrow N_2 + O$	$3 \times 10^{-12}$	(DASA, 1967)	(R32)
	$NO \rightarrow O^+ + N_2$	$1 \times 10^{-12}$	(DASA, 1967)	(R33)
$O^+$ +	$N_2 \rightarrow NO^+ + N$	$1 \times 10^{-12}$	(Schmeltekopf et al., 1968)	(R34)
	$O_2 \rightarrow O + O_2^+$	$2 \times 10^{-11}$	(Dunkin et al., 1968)	(R35)
	$NO \rightarrow O + NO^+$	$1.3 \times 10^{-12}$	(Goldan et al., 1966)	(R36)
$O_2^+$ +	$N \rightarrow NO^+ + O$	$1.8 \times 10^{-10}$	(Goldan et al., 1966)	(R37)
	$NO \rightarrow NO^+ + O_2$	$8 \times 10^{-10}$	(Goldan et al., 1966)	(R38)
	$N_2 \rightarrow NO^+ + NO$	$1 \times 10^{-17}$	(Feldman et al., 1971b)	(R39)

\* Rates given at 300 °K unless otherwise noted.

TABLE 2 (Continued)

Reaction	* Reaction Rate (cm <sup>3</sup> /sec)	Reference	
$N_2^+ + e \rightarrow N(^2D) + N$	$2.8 \times 10^{-7} (T/300)^{-0.2}$	(Mehr and Biondi, 1969)	(R40)
$O_2^+ + e \rightarrow O(^1D) + O$	$2.1 \times 10^{-7} (T/300)^{-0.7}$	(Feldman et al., 1971a)	(R41)
$O_2^+ + e \rightarrow O(^1S) + O$	$2.2 \times 10^{-8} (T/300)^{-0.7}$	(Feldman et al., 1971a; Donahue et al., 1968b)	(R42)
$NO^+ + e \rightarrow N(^2D) + O$	$3 \times 10^{-7} (T/300)^{-1.0}$	(DASA, 1967)	(R43)
$NO^+ + e \rightarrow N + O$	$1 \times 10^{-7} (T/300)^{-1.0}$	(DASA, 1967)	(R44)
$O^+ + e + M \rightarrow O + M$	$1 \times 10^{-26} (T/300)^{-2.5}$	(DASA, 1967)	(R45)
$N^+ + e + M \rightarrow N^* + M$	$1 \times 10^{-26} (T/300)^{-2.5}$	(DASA, 1967)	(R46)

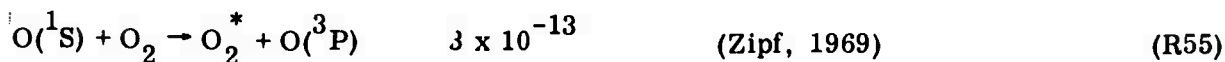
Radiative and chemical processes also involve the neutral species excited or formed by the electron beam:

Reaction	* Reaction Rate (cm <sup>3</sup> /sec)	Reference	
$N(^2D) + O_2 \xrightarrow{\dagger} NO + O$	$6 \times 10^{-12}$	(Nicholet, 1965; Black, 1969)	(R47)
$N + O_2(a^1\Delta_g) \rightarrow NO + O$	$3 \times 10^{-15}$	(Hunten and McElroy, 1968; Clark, 1970)	(R48)
$N + O_2 \rightarrow NO + O$	$2.4 \times 10^{-12} \exp(-690/T)$	(Kaufman, 1969)	(R49)
$N + NO \rightarrow N_2 + O$	$1.5 \times 10^{-12} T^{1/2}$	(Feldman et al., 1971b)	(R50)
$O + NO \xrightarrow{\dagger} NO_2 + h\nu$ (green continuum)	$6.4 \times 10^{-17}$	(Fontijn et al., 1964)	(R51)

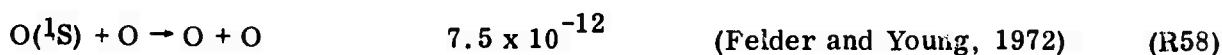
\* Rates given at 300 °K unless otherwise noted.

<u>Reaction</u>	<u>Reaction Rate</u> <u>(cm<sup>3</sup>/sec)</u>	<u>Reference</u>	
$N(^2D) \rightarrow N + h\nu$ (5199A)	$\tau = 10^5$ sec	(Wiese et al., 1966)	(R52)
$O(^1S) \rightarrow O(^1D) + h\nu$ (5577A)	$\tau = 0.74$ sec	(Wiese et al., 1966)	(R53)
$O(^1D) \rightarrow O(^3P) + h\nu$ ( $\begin{smallmatrix} 6300A \\ 6334A \end{smallmatrix}$ )	$\tau = 110$ sec	(Wiese et al., 1966)	(R54)

Competing with these radiative transitions are collisional deactivation reactions



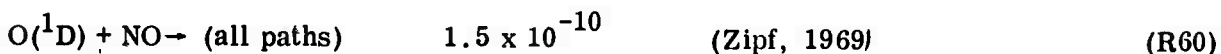
and



For large NO concentrations, as observed during auroral activity (Zipf et al., 1970), the following quenching reactions are also important:



and



These reactions, however, do not play an important role in the NASA electron beam experiment where the ambient atmosphere was quiescent with low NO concentrations. Three-body reactions are very slow for altitudes above 100 km, and are not included.

Diffusion and heating can play an important part in the chemical processes. The effect of diffusion is to dilute the concentration of the excited species and to slow down the reactions between two excited species. The change in concentration of species M due to molecular diffusion in Equation (13) is treated as an axisymmetric two-dimensional problem. The diffusion coefficient,  $D$ , determined by Kenneshea and Zimmerman (1970b), is shown in Figure 4. The shaded portion of the curve represents the eddy diffusion region which is generally observed below 106 km. Above this altitude, the diffusion becomes dominated by molecular transport. A more complicated diffusion coefficient affects dissociative-recombination processes, Reactions (R33) through (R37). Here, the diffusion involves two charged species. Hence coulomb attraction and the effects of the geomagnetic field must also be taken into account.

Electron beam heating of the irradiated region has been evaluated by accounting for the energy deposition when one ion pair is formed. This energy is distributed in heating, dissociation, excitation, and radiation. A detailed evaluation of heating rates requires calculation of the electron cooling rate, the chemical reaction rates, and the radiative emission. Since this is a substantial task, the heating rate is crudely estimated for the atmospheric dose levels in the NASA experiments. The energy deposition leading to heating the atmosphere is estimated to be 2/3 of the 35 eV required for

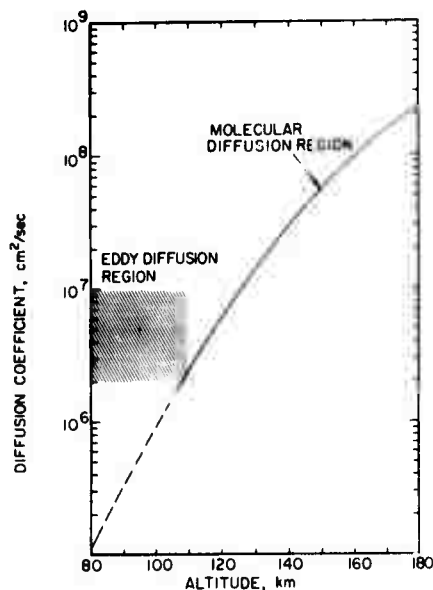


Figure 4. Diffusion Coefficient at Different Altitudes (Taken From Keneshea and Zimmerman (1970))



ion formation. The remaining third of the energy is assumed to be either used in dissociation or radiated away. For the conditions of the NASA experiment, this gives a temperature rise of about  $1^{\circ}\text{K}$ . Since this rise is small, more detailed calculations have not been considered.

## SECTION 5

### APPLICATION OF THE MODEL TO NASA "ARTIFICIAL AURORA" EXPERIMENT

In this section, the model developed in the previous two sections is employed to analyze the NASA "artificial aurora" experiment. We shall determine the extent of the electron irradiated region and compute the chemical and radiative processes that take place in the atmosphere.

The ionized region in the NASA experiment is a cylindrical volume lying along the geomagnetic field. Near the electron gun, the beam width is narrow, becoming widest in the region of maximum energy deposition. The ion pair formation rate per unit volume of atmosphere, calculated from Equations (2) and (10) for  $E_0 = 8.7$  keV and  $I = 0.49$  A, is shown in Figure 5. The altitude of the electron beam accelerator was taken to be 250 km, although this is not a critical figure as very little energy is deposited above 200 km. The number density,  $n(s)$ , was based on the 1962 Standard Atmosphere.

Since each electron in the beam slows down within several milliseconds, the atmosphere is effectively at rest during the energy deposition by an electron. The total ionization per unit volume, which depends on the irradiation by many electrons, however, does depend on the motion of the electron accelerator and the atmosphere, the time in which the electron gun is on and the size of the electron cloud.

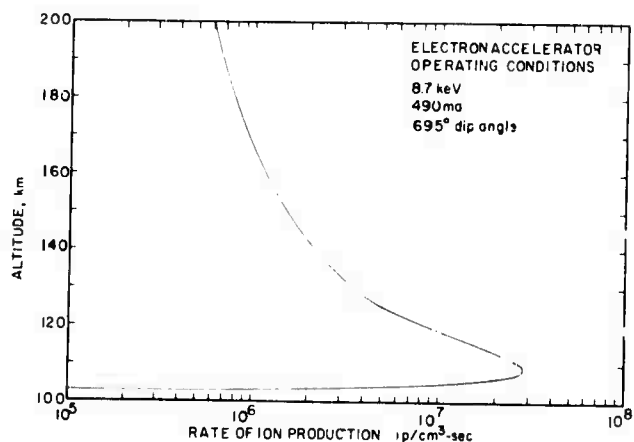


Figure 5. Ion Production Rate With Respect to Altitude Calculated for Conditions of the NASA Experiment

The observed size of the irradiated region depends also upon the type of observation. That is, optical measurements of prompt emission spectra would indicate a small cloud size, whose lateral spread is due only to the electron beam multiple scattering. On the other hand, the size determined from measuring the emission of metastable species such as  $O(^1S)$ , which have long lifetimes compared to the electron beam pulse, would appear much larger. Since the emission from  $O(^1S)$  persists much after the irradiation time, the observed cloud size includes not only the lateral spread due to electron scattering, but a wake of emitting air left by the moving electron beam.

The time  $\tau$  that a point is irradiated for a continuously operating beam is

$$\tau = \frac{S_{\perp}}{v_{\perp}} \quad (17)$$

where  $S_{\perp}$  is the lateral spread of the excited cloud (about 74 meters) and  $v_{\perp}$  is the component of the electron gun velocity perpendicular to the geomagnetic field. The latter is given by the vector equation

$$\vec{v}_{\perp} = \frac{\vec{B} \times (\vec{v} \times \vec{B})}{B^2} = \frac{\vec{v} - (\vec{v} \cdot \vec{B}) \vec{B}}{B^2} = \vec{v} - \left(\frac{v}{B}\right) \cos \theta \vec{B} \quad (18)$$

where

$$\cos \theta = \frac{(\vec{v} \cdot \vec{B})}{vB}$$

In terms of the rocket trajectory

$$\cos^2 \theta = \cos^2 \gamma - \left[ v_H \cos(90 - \alpha + \beta) - v_V \sin(90 - \alpha + \beta) \right]^2 \frac{\cos^2 \gamma}{v^2} \quad (19)$$

Here,  $v_H$  and  $v_V$  are the horizontal and vertical components of the vehicle velocity calculated from the apogee and range of the rocket;  $\alpha = 97^\circ$  is the azimuth of the rocket trajectory with respect to true north;  $\beta = -8^\circ$  and  $\gamma = 69.5^\circ$  are the declination and inclination of the geomagnetic field. Note that at apogee, where  $v_V = 0$ , Equation (19) reduces to

$$\theta = \cos^{-1} \sin(-15^\circ) \cos 69.5^\circ = 95^\circ \quad (20)$$

The velocities across field lines,  $v_\perp$ , for the four visible pulses (numbers 11 and 21 of the first two pulsing sequences) are presented in Table 3.

TABLE 3

VELOCITY ACROSS MAGNETIC FIELD LINES

	MEASURED AT		MEAN BETWEEN FRANKLIN CITY AND IGOR	CALCULATED
	FRANKLIN CITY	IGOR		
Pulse 1	98	68.6	84	110
Pulse 2	132	134	133	131
Pulse 3	160	187	173	154
Pulse 4	149	224	187	178

These velocities were determined from observations of the irradiated region from Igor and Franklin City. Notations were made of the angular velocity of the cloud, the distance from the irradiated region to the observation post, and the angle made between the line-of-sight with the direction of motion of the electron beam. These observed velocities are presented together with the velocities using Equation (22) with the horizontal and vertical components of the accelerator velocity derived from the accelerator trajectory. A sketch of the motion

of the electron-beam-excited cloud is shown in Figure 6. The irradiated region is approximately cylindrical in shape with a diameter of 74 meters and a velocity of  $v_{\perp}$ . As seen in Figure 6, Region A is illuminated for the maximum time that the atmosphere can be irradiated by the electron. Neglecting air motion, this time corresponds to 0.67, 0.56, 0.48, and 0.41 sec for the four brightest pulses respectively. The total apparent width of the irradiated air shown by the distance B on Figure 6 is

$$S_{\perp}(\text{apparent}) = S_{\perp} + v_{\perp} \tau_A \quad (21)$$

where  $\tau_A$  is the afterglow duration after beam shutdown, 0.38 sec. If winds are again neglected, this apparent width becomes 112, 123, 129, and 141, respectively, for the four brightest pulses. Depending on wind direction, atmospheric winds may either increase or decrease this irradiation time. If the wind is blowing in the same direction as the motion of the electron beam accelerator, the apparent width of the irradiated cloud becomes

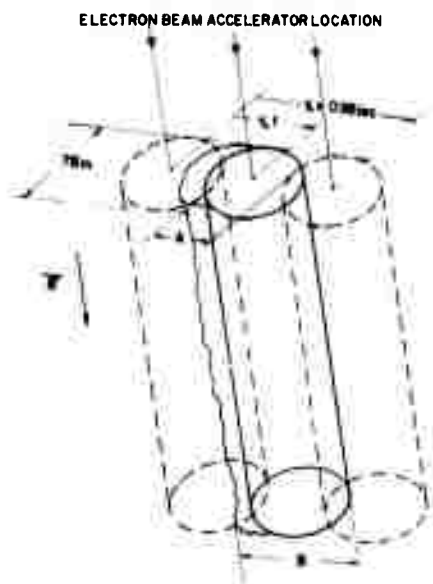


Figure 6. Sketch of the Electron Irradiated Region as the Electron Accelerator Moves Through the Atmosphere

$$S_{\perp}(\text{apparent}) = S_{\perp} + (v_{\perp} - v_A) \tau_A \quad (22)$$

where  $v_A$  is the component of atmospheric velocity parallel to  $v_{\perp}$ .

The atmospheric emission produced by electron beam irradiation can be divided into two parts; (1) prompt (short lifetime) and (2) afterglow (long lifetime) radiation.

The prompt radiation in the NASA observations was from the  $N_2^+(1-)$ ,  $O_2^+(1-)$ , and  $N_2(1+)$  bands

as produced by Reactions (R8), and (R15), respectively. The emission from these sources is shown in Figure 7 as a function of altitude. Since the radiative lifetimes of these sources are very short compared to the electron irradiation time, their radiation remains essentially constant over the electron beam pulse. The upper scale in Figure 7 gives the emission integrated through the irradiated region along the line-of-sight. The path length through the cloud was taken to be 100 meters, corresponding to line-of-sight through the 74 meter wide cloud at 108 km altitude when seen from the ground at Franklin City. The dashed line represents the combined brightness of all the prompt radiation sources, and the dotted line represents the emission from these radiators when corrected for instrument sensitivity. Note that the combined brightness of these sources exceeds 1 kilorayleigh between 104 and 132 km. This is in agreement with measured results presented in Table 1.

Other intense prompt radiation bands, such as the  $N_2$  second positive and the Lyman-Birge-Hopfield bands, are also excited by the electrons. For an extensive list of these radiators, see Chamberlain (1961). Only the radiation which falls within the bandwidth of the NASA detectors, however, are treated in this section.

The radiation from  $O(^1S)$  and  $O(^1D)$  metastable species also contribute to the observed signal.

The intensities of these radiators are plotted as a function of time for 106, 110, and 120 km in Figures 8,

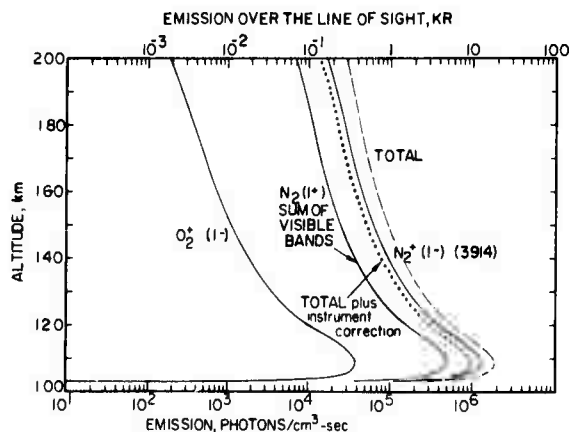


Figure 7. Steady-State Emission Levels From Prompt Radiators in the 3500 to 8000 Å Region

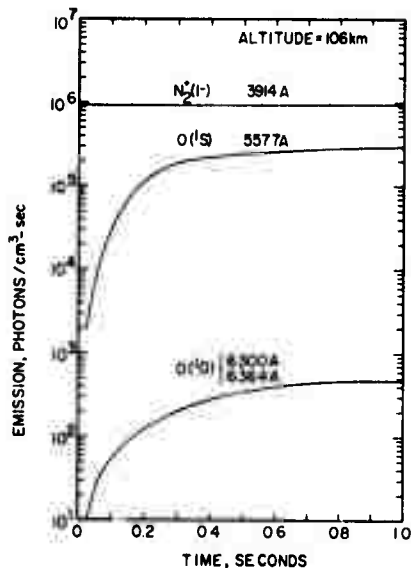


Figure 8. Calculated Emission Intensities From  $O(^1S)$  and  $O(^1D)$  During Electron Irradiation at 106 km Altitude

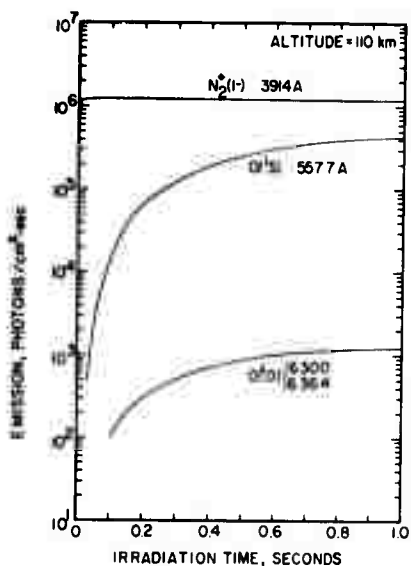


Figure 9. Calculated Emission Intensities From  $O(^1S)$  and  $O(^1D)$  During Electron Irradiation at 110 km Altitude

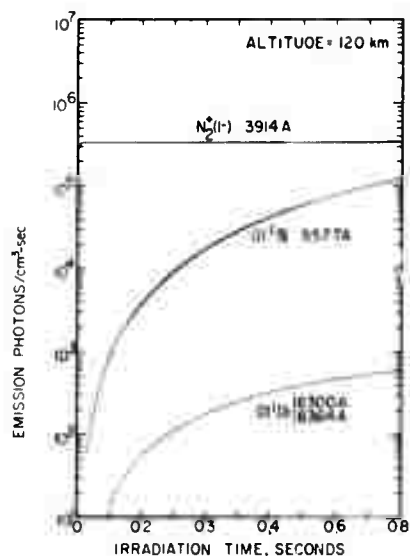


Figure 10. Calculated Emission Intensities From  $O(^1S)$  and  $O(^1D)$  During Electron Irradiation at 120 km Altitude

9, and 10 respectively. The prompt 3914Å signal from the  $N_2^+(1-)(00)$  transition is also plotted in these figures for comparison.

These intensities were calculated from the mean energy deposition rate at each altitude. It should be noted that the electron irradiation is not uniform throughout the cloud, but instead, is more concentrated near the beam axis. However, even though the chemistry changes with the variation of dose rate, the total effect is somewhat averaged out over the width of the cloud.

The emission from  $O(^1S)$  and  $O(^1D)$  is seen to increase with irradiation time. This emission may continue to increase even after the irradiation due to the continuation of dissociative-recombination reactions which are a source of these states. While the emission from directly excited prompt radiators quickly drops to zero when the irradiation ceases, these metastable states continue to emit radiation for several seconds. The  $O(^1S)$ , which accounts for a major part of this radiation, is produced in Reactions (R10), (R11), (R17), and (R42), and is depleted by radiation (R53) and quenching (R58). The emission in the afterglow is presented in Figures 11, 12, and 13, for altitudes of 106, 110, and 120 km, respectively. These signals were calculated for an irradiation time of 0.67 sec, corresponding to the maximum irradiation time of 0.41 sec were also carried out and showed the same general shape with only slightly lower initial intensities.

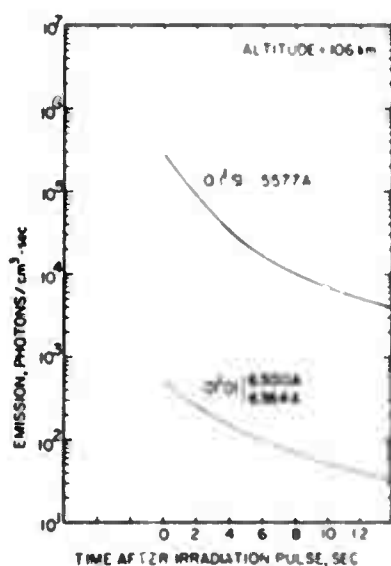


Figure 11. Emission Intensity of Afterglow Radiation From  $O(^1S)$  and  $O(^1D)$  After 0.67 Sec Irradiation Time, 106 km Altitude

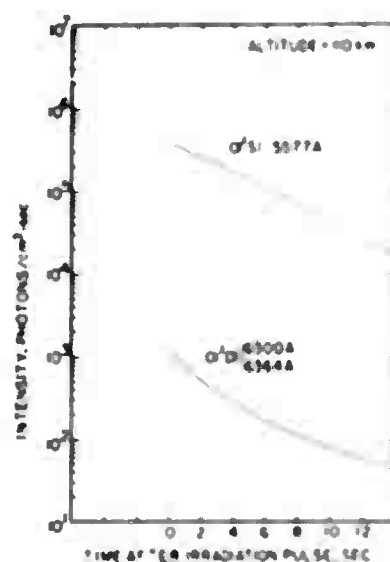


Figure 12. Emission Intensity of Afterglow Radiation From  $O(^1S)$  and  $O(^1D)$  After 0.67 Sec Irradiation Time, 110 km Altitude



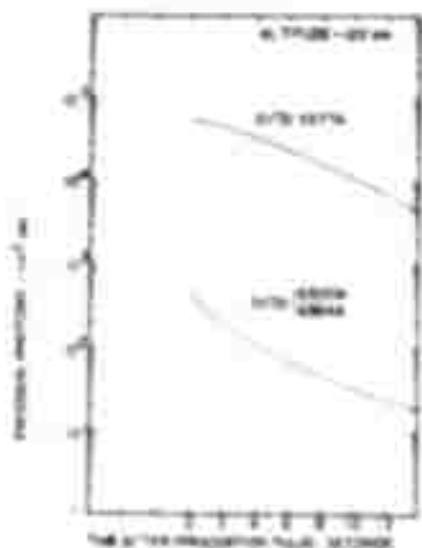


Figure 13. Emission Intensity of Afterglow Radiation From  $O(^1S)$  and  $O(^1D)$  After 0.67 Sec Irradiation Time, 120 km Altitude

Since there are no laboratory measurements for the direct production of  $O(^1S)$  from dissociative-excitation or dissociative-ionization, these cross sections were neglected in the estimate of the afterglow signal. The principle method of  $O(^1S)$  production was thus assumed to be from recombination of  $O_2^+$ . In order for the direct dissociative-excitation of  $O_2$  to contribute to the  $O(^1S)$  signal with the same intensity as that from  $O_2^+$  recombination, its cross section must be  $10^{-16} \text{ cm}^2$ , nearly the same as the total cross section for dissociation. This value of the cross section was also found by

Parkinson et al. (1970b) as necessary to explain the  $O(^1S)$  signal in auroras. A lower limit for this cross section was used in the calculations presented here. This cross section,  $1.5 \times 10^{-19} \text{ cm}^2$ , has been found by Mumma and Zipf (1971) following the 1217A ultraviolet emission from dissociative-excitation into the  $O(^1P^0)$ .

Reactions (R11) and (R17) are also possible sources of  $O(^1S)$ . The cross section for direct excitation of  $O(^3P)$ , Reaction (R11), as calculated by Henry et al. (1969) is too small to account for significant  $O(^1S)$  production. While no rate constant has been measured for  $O(^1S)$  formation from the  $N_2(A)$  state, the maximum quenching coefficient of  $N_2(A)$  by atomic oxygen (Zipf, 1969) is insufficient to account for the  $O(^1S)$  production. The contributions from each of these possible mechanisms for  $O(^1S)$  production is illustrated in Figure 14, where the irradiation time was taken

to be 0.67 sec. The maximum rate for each process is illustrated by the solid lines. The total emission from  $O(^1S)$  using a dissociative-excitation cross section of  $1.5 \times 10^{-19} \text{ cm}^2$  is shown by the solid  $O_2^+$  recombination line. The dashed line represents the emission when this cross section is  $10^{-16} \text{ cm}^2$ . The total emission using this cross section is shown by the dot-dashed line.

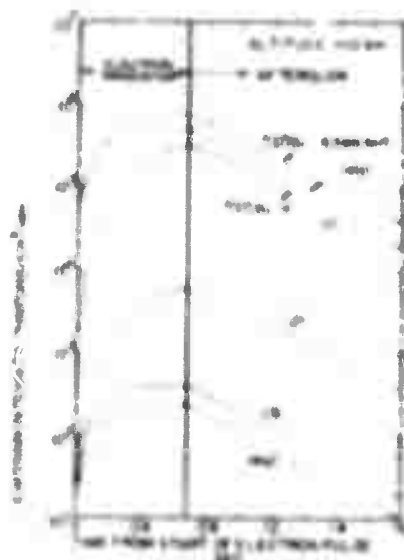


Figure 14. 5577 Å OI Emission for  $O(^1S)$  Produced by:

- |   |   |
|---|---|
| (1) $O_2^+ + e \rightarrow O + O(^1S)$    | (4) $O_2 + e \rightarrow O + O(^1S) + e$    |
| (2) $O + N_2(A) \rightarrow O(^1S) + N_2$ | Case (a) for $\sigma = 1.5 \times 10^{-19}$ |
| (3) $O + e \rightarrow O(^1S) + e$        | Case (b) for $\sigma = 1 \times 10^{-16}$   |

## SECTION 6

# DISCUSSION AND CONCLUSIONS

Even though the data obtained from the NASA Artificial Aurora experiment were limited, they allowed us to derive several important results concerning the effect of electron bombardment of the upper atmosphere. The size, shape, and altitude dependence of the observed signal gave some insight to how electrons deposit their energy into the atmosphere and the upper atmospheric chemistry involved in a disturbance by energetic electrons.

The electron slow-down in the upper atmosphere has been modeled by a simple attenuation process by fitting Equation (1) to the altitude dependent atmospheric number density. The size and shape of the cloud has also been modeled. The electron interaction with the atmosphere was modeled by fitting the energy distribution as measured in the laboratory to a varying density. The radial spread of the irradiated region was calculated by replacing the electron mean-free-path by the electron Larmor radius. The resulting electron interaction using this technique was consistent with the results of Berger et al. (1970).

In the NASA experiment, the size and shape of the cloud were determined from measurements of visible light emission. In order to interpret the data, both the interaction of electrons with the atmosphere and the resulting chemistry and radiation have been calculated. This visible emission consisted of essentially two classes of signals: prompt (short lifetime) radiation which disappears in less than a millisecond after beam turn-off, and long-lifetime radiation from metastable states whose radiation persisted for several tenths of a second after beam turn-off. The width of the observed column has been determined by combining the radiation temporal distribution, the instrument response, and the motion of the electron beam accelerator. While the data

taken during the NASA experiment shows too much scatter to infer an exact cloud width, the calculated cloud sizes agree with the experimental observations within experimental error.

The motion of the electron beam accelerator determined the air irradiation time. Atmospheric winds, which have not been considered, would move neutral species in and out of the irradiated region and complicate the analysis. The effect of winds on neutral species is to increase or decrease their interaction time with the electron beam. The electrons, on the other hand, are trapped by the magnetic field, and are affected by the atmospheric motion only through their attraction to the ions. The ions are dragged by collision with neutral species, and by coulomb attraction to the electrons. Thus, including atmospheric motion in the analysis would change the afterglow signal due to metastables, while the prompt radiation would remain essentially unchanged.

The chemistry involved in the electron beam excitation yields interesting results even from the limited data available. Detailed study of the afterglow signal from the NASA Artificial Aurora determined the amount of  $O(^1S)$  produced. While the prompt radiation signal consists of the sum of  $N_2^+(1-)$ ,  $N_2(1+)$ , and  $O_2(1-)$  bands, the main contributor to the afterglow is  $O(^1S)$ . Other metastable radiators in the visible include  $N(^2D)$  and  $O(^1D)$  which have much longer radiative lifetimes and thus contribute insignificantly to the total emitted signal. Analyzing the data available, as discussed in the previous section, leads to the conclusion that the  $O(^1S)$  production can be attributed primarily to the dissociative-recombination of  $O_2^+$ .

As seen from Figures 8, 9, and 10, the total  $O(^1S)$ , 5577A signal may build up to over one third of the  $N_2^+(1-)$  3914A signal within one second of irradiation, in agreement with what has been observed in auroras. The additional contributions of the ( $v' = 0$ ,  $v'' = 1$ ) and higher vibrational bands of  $N_2(1+)$  bands, as well as the  $O_2(1-)$  band, however, make the  $O(^1S)$  signal much lower than the prompt radiation signal. This  $O(^1S)$  signal, when corrected for instrument sensitivity, is consistent with the NASA observations.

The model developed in this report for calculating the visible emission from electron beam excitation shows good agreement with observed results. While these calculations were used to analyze the NASA experiment performed in 1969, the same techniques should be valid for predicting the results of similar types of atmospheric disturbances including future electron beam experiments.

## REFERENCES

- Anderson, R., "A Compilation of Measured Lifetimes of Gaseous Diatomic Molecules," Atomic Data, 3, 227-240, 1971.
- Black, G., T.G. Slanger, G.A. St. John, and R.A. Young, "Vacuum-Ultraviolet Photolysis of  $N_2O$ , 4 Deactivation of  $N(^2D)$ ," J. Chem. Phys., S1, 116, 1969.
- Chamberlain, J.W., Physics of the Aurora and Airglow, Academic Press, New York, 1961.
- Borst, W.L., and E.C. Zipf, "Cross Section for Electron-Impact Excitation of the (0,0) First Negative Band of  $N_2^+$  From Threshold to 3 keV," Phys. Rev., A1, 834, 1970a.
- Borst, W.L., and E.C. Zipf, "Excitation of  $O_2^+$  First Negative Bands by Electron Impact on  $O_2$ ," Phys. Rev., A1, 1410, 1970b.
- Borst, W.L., and E.C. Zipf, "Energy Spectra of Metastable Oxygen Atoms Produced by Electron Impact Dissociation of  $O_2$ ," Phys. Rev., A4, 1, 1971.
- Berger, M.J., S.M. Seltzer, and K. Marda, "Energy Deposition by Auroral Electrons in the Atmosphere," J. Atm. and Terr. Phys., 32, 1015-1045, 1970.
- Chen, J.C.Y., "Theory of Subexcitation Electron Scattering by Molecules: II: Excitation and De-Excitation of Molecular Vibration," J. Chem. Phys., 40, 3513, 1964.
- Clark, I.D., and R.P. Wayne, Proc. Roy. Soc., A316, 539, 1970.
- Cohn, A., and G. Caledonia, "Spatial Distribution of the Fluorescent Radiation Emission Caused by an Electron Beam," J. Applied. Phys., 41, 3767-3775, 1970.
- DASA Reaction Rate Handbook, July 1967, DASA, 1967.

### References (Cont.)

- Davis, T.N., T.J. Hallinan, M.C. Trichel, and W.N. Hess, "Ground-Based Optical Observations of Artificial Auroras Generated With a Rocket-Borne Electron Accelerator," Report UAG R-210, Geophysical Institute, Univ. of Alaska College, 1970.
- Davis, T.N., T.J. Hallinan, G.D. Mead, J.M. Mead, M.C. Trichel, and W.N. Hess, "Artificial Aurora Experiment: Ground-Based Optical Observations," J. Geophys. Res., 7S, 25, 6082-6092, 1971.
- Donahue, T.M., "On the Ionospheric Conditions in the D Region and Lower E Region," J. Geophys. Res., 71, 2237, 1966.
- Donahue, T.M., "Ionospheric Composition and Reactions," Science, 159, 429, 1968a.
- Donahue, T.M., T. Parkinson, E.C. Zipf, J.P. Doering, W.G. Fastie, and R.E. Miller, "Excitation of the Auroral Green Line by Dissociative Recombination of the Oxygen Molecular Ion-Analysis of Two Rocket Experiments," Planet. Space Sci., 16, 737, 1968b.
- Donahue, T.M., E.C. Zipf, and T.D. Parkinson, "Ion Composition and Ion Chemistry in an Aurora," Planet. Space Sci., 18, 171, 1970.
- Donahue, T.M., "Ionosphere, D and E Regions," EOS, 52, 513, 1971.
- Dunkin, D.B., F.C. Fehsenfeld, A.L. Schmeltekopf, and E.E. Ferguson, "Ion Molecule Reaction Studies from 300 to 600 °F in a Temperature-Controlled Flowing Afterglow System," J. Chem. Phys., 49, 1365, 1968.
- Felder, W., and R.A. Young, "Quenching of  $O(^1S)$  by  $O(^3P)$ ," J. Chem., 56, 6028, 1972.
- Feldman, P.D., J.P. Doering, and J.H. Moore, "Rocket Measurement of the Secondary Electron Spectrum in an Aurora," J. Geophys. Res., 76, 1738, 1971a.

## References (Cont.)

- Feldman, P.D., J.P. Doering, and E.G. Zipf, "Excitation of  $O^1S$  Atoms in the Day Airglow," J. Geophys. Res., **76**, 13, 3087-3094, 1971b.
- Fontijn, A., C.B. Meyer, and H.I. Schiff, "Absolute Quantum Yield Measurements on the NO-O Reaction and Its Use as a Standard for Chemiluminescent Reactions," J. Chem. Phys., **40**, 64, 1964.
- Goldan, P.D., A.L. Schmeltekopf, F.C. Fehsenfeld, H.I. Schiff, and E.J. Ferguson, "Thermal Energy Ion-Neutral Reaction Rates II. Some Reactions of Ionospheric Interest," J. Chem. Phys., **44**, 495, 1966.
- Grün, A.E., Z. Naturforsch., **12a**, 89, 1957.
- Henry, R.J.W., P.B. Burke, and A.L. Sinfailam, "Scattering of Electrons by C, N, O,  $N^+$ ,  $O^+$ , and  $O^{++}$ ," Phys. Rev., **178**, 218, 1969.
- Hess, W.N., M.C. Trichel, T.N. Davis, W.C. Beggs, G.E. Kraft, E. Stassinopoulos, and E.J.R. Maier, "Artificial Aurora Experiment and Principal Results," J. Geophys. Res., **76**, 25, 6067-6081, 1971.
- Hunten, D.M., and M.B. McElroy, "Metastable  $O_2(^1\Delta)$  as a Major Source of Ions in the D Region," J. Geophys. Res., **73**, 2421, 1968.
- Kaufman, F., "Elementary Gas Reactions," Annual Review of Physical Chemistry, **20**, 45, 1969.
- Keneshea, T.J., R.S. Narcisi, and W. Swider, Jr., "Diurnal Model of the E Region," J. Geophys. Res., **75**, 845, 1970a.
- Keneshea, T.J., and S.P. Zimmerman, "The Effect of Mixing Upon Atomic and Molecular Oxygen in the 70-170 km Region of the Atmosphere," J. Atmos. Sci., **27**, 5, 831-840, 1970b.
- Kieffer, L.J., and G.H. Dunn, "Electron Impact Ionization Cross Section Data for Atoms, Atomic Ions, and Diatomic Molecules: I: Experimental Data," Reviews of Modern Physics, **38**, 1, 1966.



### References (Cont.)

- Landshoff, R. K., J. L. Magee, and H. A. Aroeste, "Thermal Radiation Phenomena - Volume 4 - Excitation and Nonequilibrium Phenomena in Air," DASA, 1917-4, 1967.
- Lin, C. L., and F. Kaufman, "Reactions of Metastable Nitrogen Atoms," J. Chem. Phys., 55, 3760, 1971.
- Meir, F. J., and M. A. Biondi, "Electron Temperature Dependence of Recombination of  $O_2^+$  and  $N_2^+$  Ions with Electrons," Phys. Rev., 181, 264, 1969.
- Mumma, M. J., and E. C. Zipf, "Dissociative Excitation of Vacuum Ultraviolet Emission Features by Electron Impact on Molecular Gases: I:  $H_2$  and  $O_2$ ," J. Chem. Phys., 55, 1661, 1971.
- Nicholet, M., "Ionospheric Processes and Nitric Oxide," J. Geophys. Res., 70, 691, 1965.
- Norton, R. B., and C. A. Barth, "Theory of Nitric Oxide in the Earth's Atmosphere," J. Geophys. Res., 75, 3903, 1970.
- Parkinson, T. D., and E. C. Zipf, "Energy Transfer From  $N_2(A^3\Sigma_u^+)$  as a Source of  $O(^1S)$  in the Aurora," Planet. Space Sci., 18, 895, 1970a.
- Parkinson, T. D., E. C. Zipf, and T. M. Donahue, "Rocket Investigation of the Auroral Green Line," Planet. Space Sci., 18, 187-198, 1970b.
- Parkinson, T. D., E. C. Zipf, and K. A. Diek, "An Observation in situ Aurora Pulsation," J. Geophys. Res., 75, 7, 1334-1338, 1970e.
- Rapp, D., P. Englander-Golden, D. D. Briglia, "Cross-Sections for Dissociative Ionization of Molecules by Electron Impact," J. Chem. Phys., 42, 4081, 1965.
- Schmeltekopf, A. L., E. E. Ferguson, and F. C. Fehsenfeld, "Afterglow Studies of Reactions  $He^+$ ,  $He(2^3S)$ , and  $O^+$  With Vibrationally Excited  $N_2$ ," J. Chem. Phys., 48, 2966, 1968.

### References (Cont.)

- Spencer, L. V., and J. Coyne, "Theory of Deep Penetration of Electrons and Charged Particles," Phys. Rev., 128, 2230, 1962.
- Stair, A. T., Jr., and H. P. Gauvin, "Research on Optical Infrared Characteristics of Aurora and Airglow," Aurora and Airglow, edited by B. M. McCormac, 365-389, Reinhold, New York, 1967.
- Stair, A. T., Private Communication, 1971.
- Stolarski, R. S., V. A. Dulock, Jr., C. E. Watson, and A. E. S. Green, "Electron Impact Cross Sections for Atmospheric Species, 2: Molecular Nitrogen," J. Geophys. Res., 72, 15, 1967.
- Strobel, D. F., "Diurnal Variation of Nitric Oxide in the Upper Atmosphere," J. Geophys. Res., 76, 2441, 1971.
- Swider, W., Jr., and R. S. Narcisi, "On the Ionic Constitution of Class I Auroras," Planet. Space Sci., 18, 379, 1970.
- Ulwick, J. G., "Rocket Measurement of Auroral Parameters in Aurora and Airglow," Aurora and Airglow, edited by B. M. McCormac, 225, Reinhold, New York, 1967.
- Winters, H. F., "Ionic Adsorption and Dissociation Cross Section for Nitrogen," J. Chem. Phys., 44, 1472, 1966.
- Wiese, W. L., M. W. Smith, and B. M. Glennon, "Atomic Transition Probabilities V1 Hydrogen Through Neon," NBS, 1966.
- Zipf, E. C., "The Collisional Deactivation of Metastable Atoms and Molecules in the Upper Atmosphere," Can. J. of Chem., 47, 1863, 1969.
- Zipf, E. C., W. I. Borst, and T. M. Donahue, "A Mass Spectrometric Observation of NO in an Auroral Arc," J. Geophys. Res., 75, 6371, 1970.